

# A Physical Model for the Polarized Scattering of Light

David Brayford<sup>1</sup>, Martin Turner<sup>2</sup>, W.T Hewitt<sup>2</sup>

<sup>1</sup>Scientific Computing and Imaging Institute, The University of Utah. <sup>2</sup>The University of Manchester

## ABSTRACT

The change in polarization state due to the interaction of light with the surface and beneath the surface of an object has become increasingly important in realistic image synthesis of materials such as metallic, iridescent and pearlescent paint, skin, hair and cosmetics. This paper presents a model for the anisotropic scattering of polarized light based upon the physics of light; which is capable of calculating both partial and complete polarization using a combination of Jones and Mueller calculus, as well as incorporating self shadowing effects.

CR Categories and Subject Descriptors: I.3.3 [Computer Graphics]: Three-Dimensional Graphics and Realism – Raytracing;

## 1 INTRODUCTION

The simulation of polarization effects to synthesize photorealistic images has until recently been generally overlooked, with a few notable exceptions [5, 8, 14, 20, 22-24]. One of the main reasons why polarization has been overlooked is the general misconception that polarization effects have a minimal contribution to the appearance of the average scene, which can in some way be accounted for by the fact that the human visual system possesses minimal sensitivity to the polarization states of the light entering the eye. However, many real world scenes display significant polarization effects from dielectric materials such as the glare from glass windows, large volumes of water, and the darkening of crystals; as well as the discolouration of metallic objects and their reflections, and some of these have been simulated in photorealistic image synthesis using the Fresnel equations [6].

The predictive simulation of the polarization states of the light that impinges upon a transparent multilayered material is important to synthesize accurate photorealistic images for materials that consist of dielectric layers such as automobile paints, coatings, optical devices and ceramics. Being able to predict the visual appearance of multilayered materials before they are manufactured, reduces costs, and improves quality by estimating the parameter tolerances.

The main focus of this paper is to investigate the use of polarization techniques described in the physics literature [10-12] for photorealistic image synthesis within the computer graphics arena. The research also covers the development of a new theoretical model for the anisotropic scattering of polarized light, including the visualization of this theoretical model, and its validation.

## 2 PREVIOUS WORK

The use of polarization to produce realistic computer generated images was first proposed by Wolff and Kurlander [24] and was extended by Tannenbaum et al. [20] to render anisotropic media. Both these models are based upon Jones calculus that has also been employed by Guy and Soler [14] to render gemstones. Another method by Freniere et al. was proposed within the optics community to model polarization within a Monte Carlo ray tracer [8]. This method uses Mueller calculus to describe polarization states. Subsequently Wilkie et al. [22] employed a similar approach to the rendering of polarization effects which he extended to model skylight polarization [23]. Previously in computer graphics, surface scattering models have attempted to simulate simple polarization effects from optically smooth surfaces using the Fresnel equations, which was proposed by

Cook and Torrance [6]. This has since been used in a simplified form by numerous applications to model dielectrics and various metals. Another more sophisticated surface scattering model proposed by He et al. [15] simulates polarization effects using vector Kirchhoff theory [3].

## 3 THE NEW SCATTERING MODEL

The new proposed scattering model is an anisotropic derivative of the polarized light scattering model originally developed by Germer et al. [11, 12]. The model is based on Mueller calculus [16]; which incorporates specular scattering from the surface of the media, as well as specular scattering from the slopes of plate like subsurface particles, and diffuse scattering from spherical subsurface particles (see Figure 1). The advantages of using Mueller calculus over Jones calculus is that it can be employed to simulate partially polarized as well as fully polarized radiation.

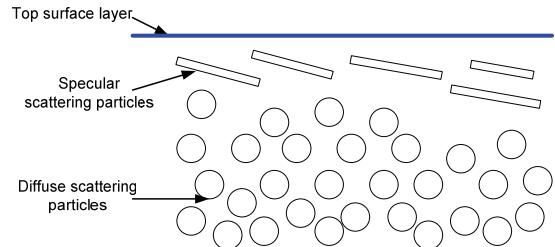


Figure 1. Schematic representation of the scattering media.

The top surface can be considered to be a coating that specularly reflects light. The large plate like particles below the surface layer, produce the specular subsurface scattering. Finally the deepest scattering layer consists of spherical subsurface particles that scatter light diffusely.

The ability to simulate a multilayered material is relatively straight forward, and involves creating a stack of individual material layers, which can be calculated in a recursive manner.

### 3.1 Surface Scattering Model

In the proposed model an anisotropic specular surface and specular subsurface scattering mechanism is derived from the model developed by Germer and Nadal [12]. The anisotropic derivations to these scattering models involve extending the existing isotropic slope distribution functions (sdf) from a mean distribution of the slope orientation that previously assumed that the distribution of slopes are uniform in all directions. In the new model the slope distribution function incorporates the mean distribution of the orientation of the slopes in both

the  $x$  and  $y$  directions, which are explicitly defined. The existing specular surface and subsurface scattering models [11, 12] contains both exponential and Gaussian slope distribution functions. The new model contains only an anisotropic Gaussian slope distribution function that is dependent upon the standard deviation of the slope orientations for both the  $x$  and  $y$  directions.

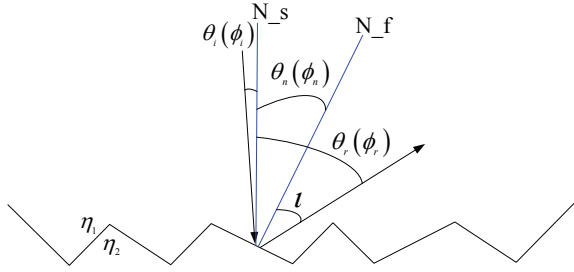


Figure 2. Scattering of light from the surface microfacets

Figure 2 illustrates the scattering of light from a surface consisting of facets where  $N_s$  is the surface normal,  $N_f$  is the facet normal, and the angle of the surface slope normal is  $\theta_n$ .

The facet scattering model was designed to model the anisotropic specular scattering of light from facets aligned on the surface of the media. That can be characterized with respect to the orientation of the slope in both the  $x$  and  $y$  directions  $(\zeta_x, \zeta_y)$ , considers the probability that the orientation of the slope in both directions is within a differential slope  $d\zeta_x d\zeta_y$ . This can be done by defining the probability that the slopes in the  $x$  orientation is between  $\zeta_x$  and  $\zeta_x + d\zeta_x$ , and the slopes in the  $y$  orientation is between  $\zeta_y$  and  $\zeta_y + d\zeta_y$ , which is referred to as the anisotropic slope distribution function (sdf),  $S(\zeta_{aniso})$ .

We can now define the Gaussian anisotropic slope distribution function, which was used within the BRDF models.

The given anisotropic Gaussian slope distribution function (sdf)  $S_{Gaussian}(\zeta_{aniso})$  is:

$$S_{Gaussian}(\zeta_{aniso}) = \frac{1}{2\pi\sigma_x\sigma_y} \exp\left[-\left(\frac{\zeta_x^2}{\sigma_x^2} + \frac{\zeta_y^2}{\sigma_y^2}\right)^{1/2}\right] \quad (1)$$

where the distribution of slopes in the  $x$  and  $y$  orientations are

$$\zeta_x = \tan \theta_n \cos \phi_n \quad (2a)$$

$$\zeta_y = \tan \theta_n \sin \phi_n \quad (2b).$$

The differential probability that a specific point having a slope is:

$$p(\zeta_x, \zeta_y) d\zeta_x d\zeta_y = S(\zeta_{aniso}) d\zeta_x d\zeta_y \quad (3)$$

We now consider the surface specular scattering for polarized light.

This involves converting a four component Jones matrix into a Mueller, using the method described by Bohren & Huffman [2, 4]. The resulting Mueller matrix is then used to determine the surface specular scattering for faceted surface. So

$$\begin{pmatrix} m_{00} & m_{01} & m_{02} & m_{03} \\ m_{10} & m_{11} & m_{12} & m_{13} \\ m_{20} & m_{21} & m_{22} & m_{23} \\ m_{30} & m_{31} & m_{32} & m_{33} \end{pmatrix} = J2M \begin{pmatrix} q_{ss} & q_{ps} \\ q_{sp} & q_{pp} \end{pmatrix} \quad (4)$$

Where  $J2M$  is the Jones to Mueller matrix conversion illustrated in equation 4.

$$\begin{aligned} q_{ss}^{surface\_specular} &= r_p(t) \sin \theta_i \sin \theta_r \sin^2 \phi_r + a_2 a_3 r_s(t) \\ q_{sp}^{surface\_specular} &= -\sin \phi_r (a_2 r_s(t) \sin \theta_r - a_3 r_p(t) \sin \theta_i) \\ q_{ps}^{surface\_specular} &= -\sin \phi_r (a_3 r_s(t) \sin \theta_i - a_2 r_p(t) \sin \theta_r) \\ q_{pp}^{surface\_specular} &= r_s(t) \sin \theta_i \sin \theta_r \sin^2 \phi_r + a_2 a_3 r_p(t) \end{aligned} \quad (5)$$

where  $q_{xy}^{surface\_specular}$  are the components of the Jones matrix.

Please refer to [11, 12] for details on underlying equations used in the BRDF models developed by Germer. Finally this model can be extended to include additional dielectric coating applied to the surface of the media as long as their optical properties are known. That is calculated using a recursive method starting at the surface air interface layer.

The anisotropic surface BRDF expressed in terms of Mueller calculus is then given by:

$$f_r^{surface\_specular} = \frac{(1 + \zeta_{aniso}^2)^2 S(\zeta_{aniso}) S_p}{[4(a_1)^2 \cos \theta_i \cos \theta_r] M(q^{surface\_specular})} \quad (6)$$

where  $S_p$  is the anisotropic shadowing function.

### 3.2 Anisotropic Surface Shadowing Function

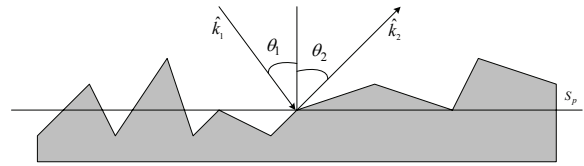


Figure 3. Illustrates the basic mean surface geometry and coordinate system that is used to calculate the shadowing function for the anisotropic specular scattering from the surface facets and the plate like subsurface particles.

For the majority of materials the surface is not optically smooth, but rather contains surface defects known as microfacets or surface roughness. The scattering of light from a rough surface can be simulated by the anisotropic surface scattering model described previously. However, this does not account for the self shadowing effects caused by the distribution of facets on the surface.

To account for the surface shadowing effects that are associated with scattering of light from rough anisotropic surfaces (see Figure 3) a version of the shadowing function developed by Sancer [18] was incorporated into the model.

$S_p$  is the probability distribution of the surface, and can be defined for the vector  $\hat{v} = \hat{k}_1 - \hat{k}_2 = (u, v, \omega)$  [19].

$$\text{if } u = v = 0 \text{ and } \theta_1 \leq \theta_2 \text{ then } S_p = \frac{1}{C_0 + 1} \quad (7a)$$

$$\text{if } u = v = 0 \text{ and } \theta_2 \leq \theta_1 \text{ then } S_p = \frac{1}{C_2 + 1} \quad (7b)$$

Where  $C_n$  is the correlation function for a Gaussian random surface.

The shadow function expressed in equation (7) has been previously used in computer graphics by Stam [19] to describe the shadowing effects from rough anisotropic surface for the simulation of diffraction effects.

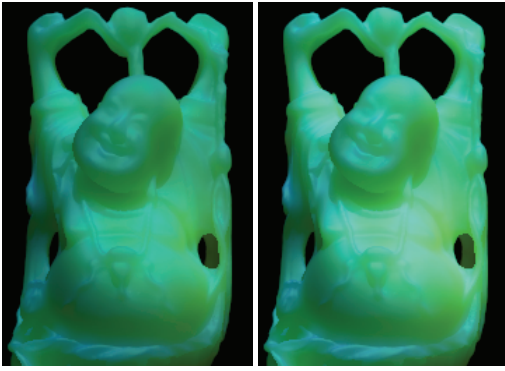


Figure 4. The rendered image on the left of Figure 4 was simulated with surface shadowing effects enabled. While the image on the right was simulated with the surface shadowing effects disabled.

Notice the slight difference in the intensity of the light scattered from the two statues in Figure 4 with the image on the left having less intense specular highlights.

### 3.3 Specular Subsurface Scattering Model

The scattering of light from the flat plate like particles beneath the surface of the transparent medium can be treated in a similar manner as the anisotropic surface scattering model described previously. However, the subsurface specular scattering model [5] as shown in Figure 5, requires the simulation of the refraction of light that occurs between the layers of the different transparent materials to be included. The difference in the methods used to calculate the surface and subsurface specular scattering models are outlined below.

The refraction of light is calculated using Snell's law [3], which gives the relationship between angles of incidence and refraction for a wave travelling through an interface between two media with different indices of refraction.

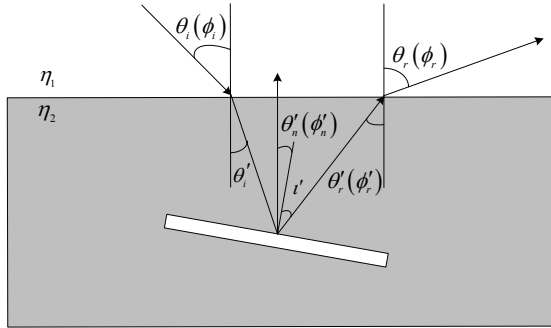


Figure 5. Scattering of light from the specular subsurface particles

The components of the Jones matrix for the subsurface specular scattering particles  $q_{\text{subsurface\_specular}}$  are described by Germer et al. [11, 12].

As with the anisotropic surface scattering model the subsurface specular scattering model is able to account for shadowing effects. The model doesn't account for the transmission of light through the surface of the subsurface particles. However, it would be relatively straightforward to extend the model to handle the transmission of light through the subsurface particles, but this would significantly increase the time it would take to calculate the BRDF.

The anisotropic subsurface specular BRDF expressed in terms of Mueller calculus is then given by:

$$f_r^{\text{subsurface\_specular}} = \frac{(1 + \zeta_{\text{aniso}}^2)^2 S'(\zeta_{\text{aniso}}) \eta^2 S_p}{[4(\alpha_1')^2 \cos \theta_i \cos \theta_r] M(q_{\text{subsurface\_specular}})} \quad (8)$$

### 3.4 Diffuse Subsurface Scattering Model

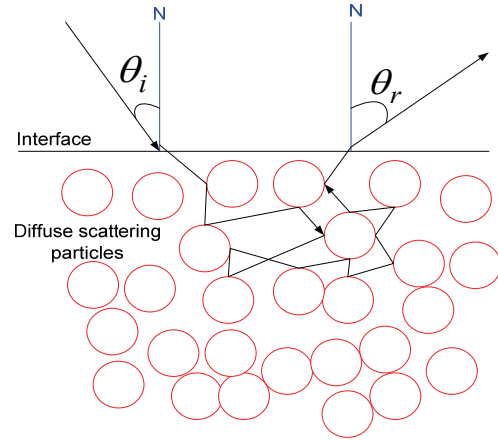


Figure 6. Diffuse subsurface scattering from spherical particles.

The diffuse scattering mechanism as shown in Figure 6, occurs when the light undergoes multiple scattering events. This mechanism results in the depolarization of the light [12], although a small amount of residual polarization occurs due to the differences between the transmission coefficients for the s and p polarization states. This diffuse scattering produces the uniform or Lambertian diffuse reflection component.

The BRDF for the scattering of light from a distribution of spherical particles is then given by:

$$f_r^{\text{diffuse\_particles}} = \frac{\alpha}{4\pi} \begin{pmatrix} f_{r0,0}^{\text{diffuse\_particle}} & f_{r0,1}^{\text{diffuse\_particle}} & 0 & 0 \\ f_{r1,0}^{\text{diffuse\_particle}} & f_{r1,1}^{\text{diffuse\_particle}} & 0 & 0 \\ 0 & 0 & 0 & 0 \\ 0 & 0 & 0 & 0 \end{pmatrix} \quad (9)$$

where  $\alpha$  is the reflectance of the diffuse scattering media, although it should be noted that this alone does not account for the media interface.

The components of the Mueller matrix  $f_{rx,y}^{\text{diffuse\_particle}}$  used in calculating the BRDF are given in [11, 12].

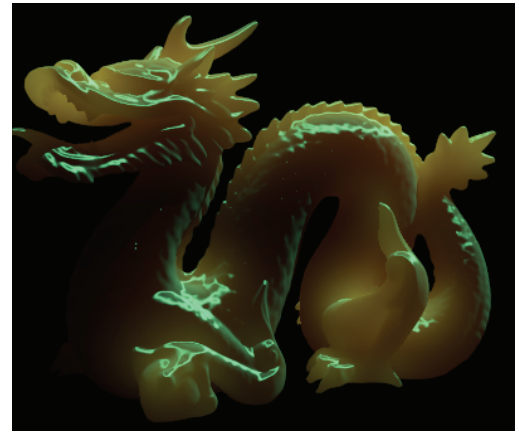


Figure 7. A translucent dragon statue that is made of a type of nephrite jade simulated using the new theoretical reflectance models for surface and subsurface diffuse scattering.

Figure 7 shows how smoothly polished the nephrite dragon statue appears, which enhances the visual realism of the image. This is due to the combination of reflectance properties from the surface scattering and the subsurface diffuse scattering of light from the material.

#### 4 COMPONENTS OF THE SCATTERING MODEL

The ratio of light which undergoes specular scattering from the surface of the material, specular scattering from subsurface particles or diffuse scattering from subsurface spherical particles is controlled by:

- The incident angle of the light that impinges upon the surface of the material.
- The wavelength of the incident light that impinges on the material.
- The wavelength dependent index of refraction of the transparent material, which is the real component of the complex index of refraction.
- The density of the subsurface particles distributed within the transparent media.
- The size of the subsurface particles, distributed within the transparent media.

It is relatively straightforward to calculate the amount of light reflected from the surface of the material and the amount of light that is transmitted into the transparent material using the Fresnel equations [16]. The specular scattering of light from the surface is expressed in the form of a BRDF  $f_r^{surface\_specular}$  and is calculated by equation (6).

##### 4.1 Combining the Scattering Models

The subsurface scattering components are defined between upper and lower limits of the particle density distribution of the specular and diffuse scattering particles, to determine the ratio of specular to diffuse scattering. Beyond these limits the model is not valid. If the ratio of specular to diffuse particle densities is close to the lower limit diffuse subsurface scattering predominates over specular subsurface scattering, resulting in a reflection hemisphere of uniform intensity. If the ratio of specular to diffuse particle densities is close to the upper limit specular subsurface scattering predominates over diffuse subsurface scattering, resulting in a reflection hemisphere with the appearance of subsurface specular highlights known as glitter or sparkles.

The contribution to the total reflectance of the material from surface and subsurface theoretical scattering models is determined by adding weighted contributions of the anisotropic surface scattering BRDF  $f_r^{surface}$  from equation (6) to the anisotropic subsurface specular BRDF  $f_r^{ss\_specular}$  from equation (8), and the subsurface diffuse BRDF  $f_r^{ss\_diffuse}$  from equation (9). Hence giving:

$$f_r = f_r^{surface} \omega_{reflected} + f_r^{ss\_specular} \omega_{specular} + f_r^{ss\_diffuse} \omega_{diffuse} \quad (10)$$

where  $\omega_{reflected}$  is the amount of light reflected from the surface of the material, which can be calculated using the Fresnel equation.  $\omega_{specular}$  is the amount of light specularly scattered from subsurface particles, which is calculated from the density of plate-like particles within the material; which was calculated from the density and scattering cross sectional area of the plate like particles.

A beam of intensity  $I$  will scatter  $dI = -I\rho\sigma dx$  photons within a distance  $dx$ , and the intensity of the light falls by this amount. Where  $\rho$  is the particle density,  $\sigma$  is the scattering cross section

for an individual plate-like particle and  $I$  is the intensity of the light.

Integrating  $\frac{dI}{I} = -\rho\sigma dx$  from  $x = 0$  to  $x = L$  we now have the exponential attenuation of the light scattered by the specular subsurface particles.

$$\omega_{specular} = I = I_0 e^{-\rho\sigma L} \quad (11)$$

where  $I_0$  is the intensity of the incident light.

$\omega_{diffuse}$  is the amount of light diffusely scattered from subsurface particles, which was calculated from the density of the spherical particles within the material.

$$\omega_{diffuse} = \frac{I_{scattered}}{I_{incident}} = \frac{N_A L \rho}{A \times 10^{-3}} \quad (12)$$

where  $N_A$  is Avogadro's constant,  $A$  is the molecular mass calculated from the periodic table of elements, and  $L$  is the target's thickness.

The research performed initially focused upon the development of a BRDF model to describe the subsurface scattering of polarized light that is based upon widely employed scientific principles and controlled by physically meaningful parameters, which was then incorporated within a lighting simulation system to generate photorealistic images. The BRDF model that has been produced combines the anisotropic version of the specular scattering of light from the surface facets and the subsurface plate-like particles with multiple scattering from the spherical subsurface particles (rendered images in Figures 8 and 21).



Figure 8. Illustrates how smoothly polished a simulated nephrite jade dragon statue appears, which enhances the soft appearance of the statue and the visual realism of the image. This is due to a combination of reflectance properties from the surface scattering, the subsurface specular and subsurface diffuse scattering of light from the material.

#### 5 IMPLEMENTATION

To enable the theoretical BRDF models to be used to generate photorealistic images. Three different open source software components required modification.

The first component was the SCATMECH C++ library [10]. This library contains the underlying polarized BRDF models, which the research was based upon. That was extended to incorporate the BRDF models described in this paper.

The next component was an interface that enables the software rendering program to access the BRDF models within the SCATMECH library. The interface was a modified version of the Modeled Integrated Scattering Tool [9] (MIST), which was

developed for the SCATMECH library by Germer. The modified MIST program performs the integration of the BRDF over solid angles specified by the renderer. The integrals generated were then converted into intensity values by the modified MIST program. The subsequent light intensity values at wavelengths within the visible spectrum were then converted into a spectral power distribution. This spectral power distribution was then converted to its corresponding CIE XYZ colour values, which is described in detail by Glassner [13]. Finally the resulting XYZ values were converted to RGB values through multiplication by a transformation matrix that is unique for a specific output colour space. The resulting RGB values and corresponding intensity values were stored within a text file, which would be used by the renderer.

The Final component was the rendering software that would generate the images. For the purposes of this research the Realistic Image Synthesis Engine (RISE) [17] raytracing software was chosen as it contains numerous useful features such as support for spectral & optical data, multiple sampling methods, photon mapping, and allows extensions to be easily incorporated. The renderer was modified to write the BRDF input parameters as a MIST input file and read in the MIST output file containing the BRDF data, which would be used to generate the image.

## 6 VALIDATION

The validation of analytical BRDF models has become an increasingly important issue in computer graphics [21]. The benefits of producing physically accurate and predictive rendering are generating interest in areas such as virtual prototyping [1], architecture, fashion design, biophysical/ biomedical models and archaeology.

The validation and implementation of the BRDF model allows for both quantitative and qualitative analysis to be performed for demanding applications. This serves as an indication of the errors incurred within the simulation by comparing the results with reference data. The validation of the new theoretical BRDF models employs two methods. The first method involves the use of spectral reflectance measurements that were obtained for translucent ski wax samples at four fixed angles using a goniospectrophotometer for wavelengths between 360nm and 750nm at intervals of 10 nm. The second method involves performing a visual difference comparison between a reference image and a rendered image using Daly's visual difference predictor [7].

### 6.1 Measurement

These methods were used to compare the spectral reflectance distribution of the measured and simulated samples as illustrated in Figures 10 and 13. These images indicate that in certain situations the correlation between the measured and simulated spectral reflection was poor. This was due to random measurement and sample presentation errors, which led to light loss from the goniospectrophotometer at the sample presentation port; and the goniospectrophotometer used to measure the reflectance requires that the sample materials consist of flat thin segments so that they can fit snugly against the aperture. If the sample material is not flat then some of the light scattered from the sample escapes into the surroundings and is not detected. One of the problem associated with obtaining reflectance measurements for flat translucent materials that are not thinly sliced, is that the light that scatters within the material can exit the material from any surface at any angle, and not all the light scattered will then be detected. The problem of light escaping from the goniospectrophotometer was a constant source of errors and could not be quantified.

Unfortunately, this loss of light from the spectrophotometer meant that the reflectance measurements could not be used for the purpose of validation. The result of this meant that we were unable to determine the physical accuracy of the model.

However, to overcome this problem we decided to use a model of the human visual system for determining image quality, which has a varying sensitivity to error that is based upon the viewing context. This means that equivalent optical discrepancies can be very obvious in one situation and imperceptible in another. For the purposes of producing photorealistic images it is ultimately the perceptibility of this error that governs image quality.

The measurements of visibility were obtained using the model of human vision captured in the visible differences predictor (VDP) developed by Daly [7]. This technique is a mixture of stochastic and deterministic algorithms used in a sequence that are optimized to reduce the differences between the intermediate and final images as perceived by a human observer in the course of lighting computation.

### 6.2 Datawax Ski Wax

The measured and simulated spectral reflectance data for the Datawax ski wax is depicted in the graph and visually compared.

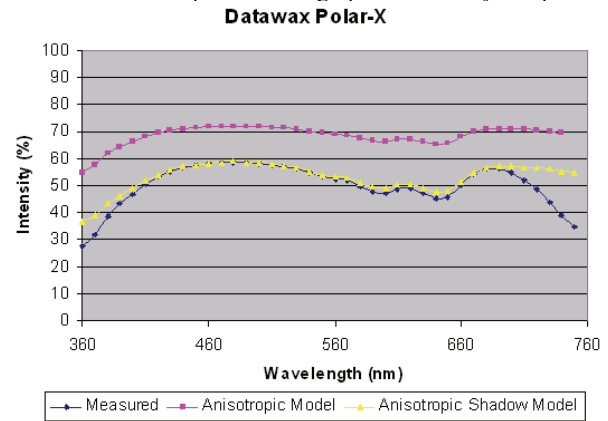


Figure 9. Shows the measured and simulated spectral reflectance for the Datawax Polar-X wax.

The spectral reflectance of the theoretical BRDF models for Datawax shown in Figure 9 follows the same trends as the measured reflectance.

The real and rendered HDR images were then compared using the VDP program.

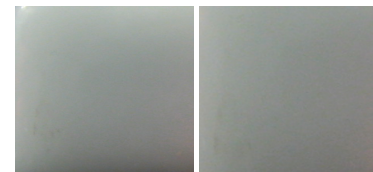


Figure 10a

Figure 10b

Figure 10. The comparison of real and rendered images of a block of Datawax using a perception based metric (VDP). Where 10a is the real image, 10b is the image generated by the anisotropic BRDF model.

The visual difference image generated from the real and rendered images of a section of Datawax as illustrated in Figure 10 has only 1.03% pixel difference greater than 75% and 0.29% difference greater than 95%. This indicates that the human visual system can only detect a slight difference between the two images. Even though there is a large difference in the reflectance

values of the measured and anisotropic BRDF model as illustrated in Figure 9.



Figure 11. A simulated dragon statue made from Datawax ski wax using isotropic reflectance model with the surface shadowing effects enabled.

### 6.3 Orange Ski Wax

The measured and simulated spectral reflectance data for the orange ski wax are depicted in the graph and visually compared.

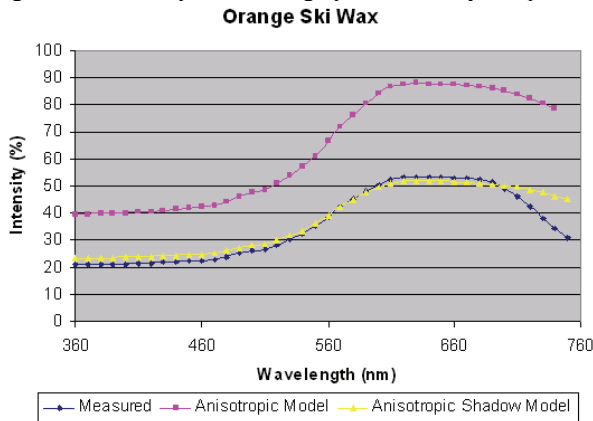


Figure 12. Shows the spectral reflectance properties generated by the theoretical BRDF models for the orange ski wax follow the same trend as the measured reflectance.

Using the same method described previously the visual difference metric can be calculated for the orange ski wax.

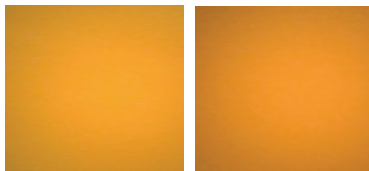


Figure 13a

Figure 13b

Figure 13. The comparison of real and rendered images of orange ski wax using VDP, where 13a is the real image, 13b is the rendered.

Although the reflectance values for the measured orange ski wax illustrated in Figure 12 are approximately twice that of the simulated anisotropic BRDF model. The visual difference image generated from the real and rendered images of the orange ski wax as illustrated in Figure 13 has a pixel difference of 1.27% greater than 75% and a pixel difference of 0.36% greater than 95%, which indicates that there is only a slight difference, which

the human visual system can detect between the image captured with the digital camera and the one generated by the ray tracer.



Figure 14. A simulated dragon statue made from orange ski wax using the isotropic reflectance model with the surface shadowing effects enabled.

## 7 RESULTS

To illustrate the effects of polarized light scattering on the appearance of a material we generated a set of images that exhibit strong specular highlights in the form of glare, and then generated the same set of images as though they are viewed through a polarizing filter.

The images depicted in Figures 15, 16 & 17 show the effects of polarization of surface and subsurface scattering from the dragon and Buddha statues. The statues in Figures 15a, 16a & 17a were viewed without a polarized filter. While the statues in Figure 15b, 16b & 17b were viewed through a polarizing filter. Notice how the glare is significantly reduced for the image in Figures 15b, 16b & 17b, which also appear clearer due to the reduction in the signal to noise ratio.

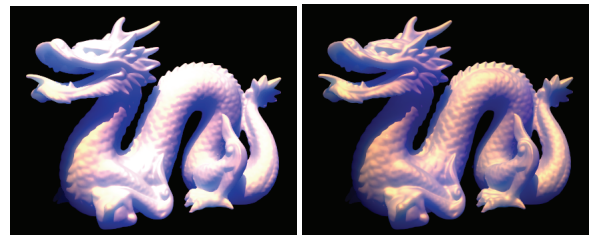


Figure 15a

Figure 15b

Figure 15. Illustrates the effects of polarization of surface and subsurface scattering from the rendered dragon statue. Figure 15a is viewed without a polarized filter while Figure 15b is viewed through a polarizing filter.

## 8 CONCLUSION

This paper introduces to computer graphics a method described in the physics literature [10-12] for the simulation of surface and subsurface scattering of polarized light, which was extended to incorporate anisotropic scattering behaviour. In addition to being able to simulate polarized light scattering the modified model can be used to simulate and predictively render new as well as existing multilayered materials.

From the initial investigation it is suggested that the effect on the polarization of the scattered light from the combination of surface and subsurface scattering, can have a significant effect upon the colour and overall appearance of the material as illustrated in Figures 15, 18 & 19. We have also shown that the addition of an anisotropic surface shadowing function to the

theoretical BRDF models enables better correlation between the reflectance values of the simulated and measured materials.

In predictive rendering it is essential that results are accurate and can be validated. In this paper we have shown that it was difficult to validate the theoretical BRDF model because acquiring accurate reflectance measurements is a complex task and should be performed by a specialist. The result of not being able to obtain accurate reflectance measurements meant that the models could not be validated for their physical accuracy.

However, it is not always possible to validate the accuracy of the rendering image generated by the models using measured data and the use of a method that is based on the sensitivity of the human visual system can in some cases provide a better method of validation for computer generated images.

Future work will focus on the validation of the new theoretical models using measured spectral reflectance measurements that will include most of the scattering hemisphere as the goniospectrophotometer used in this research could only obtain reflectance measurements from thin flat surfaces with a fixed incident angle and four fixed scattering angles.

## 9 ACKNOWLEDGEMENTS

The authors would like to thank the creators of the SCATMECH library [10] and the RISE spectral renderer [17] and Huw Owens (the University of Manchester) for his helpful suggestions and discussions on scattering and for the use of a goniospectrophotometer. Finally I would like to thank the School of Computer Science at the University of Manchester for funding my PhD.

## REFERENCE

- [1] "RealReflect Project," January 2006.
- [2] C. F. Bohren and D. R. Huffman, *Absorption and Scattering of Light by Small Particles*, 1983.
- [3] M. Born and E. Wolf, *Principles of Optics, Electromagnetic Theory of Propagation, Interference and Diffraction of Light*, 7 ed: Cambridge University Press, 1999.
- [4] D. Brayford, "Rendering of Polarized Subsurface Light Scattering," in *Computer Science*, vol. PhD: The University of Manchester, 2006.
- [5] D. Brayford, M. Turner, and W. T. Hewitt, "A Physical Based Spectral Model for Polarized subsurface Light Scattering," in *13th Pacific Conference on Computer Graphics and Applications (PG'05)*. Macao, China, 2005, pp. 25-27.
- [6] R. L. Cook and K. E. Torrance, "A Reflectance Model for Computer Graphics," *ACM Transactions on Graphics*, vol. 1, pp. 7-24, 1982.
- [7] S. Daly, "The visible differences predictor: an algorithm for the assessment of image fidelity," in *digital images and human vision*, 1993, pp. 179-206.
- [8] E. R. Freniere, G. G. Gregory, and R. A. Hassler, "Polarization Models for Monte Carlo Ray Tracing," *Optical Design and Analysis Software, Proceedings of SPIE*, vol. 3780, 1999.
- [9] T. A. Germer, "Modeled Integrated Scattering Toolkit (MIST)," 1.0 ed, 2004.
- [10] T. A. Germer, "SCATMECH: Polarized Light Scattering C++ Class Library," 5.01 ed, 2005.
- [11] T. A. Germer and E. Marx, "Ray Model of Light Scattering by Flake Pigments or Rough Surfaces with Smooth Transparent Coatings," *Applied Optics*, vol. 43, pp. 1266-1274, 2004.
- [12] T. A. Germer and M. E. Nadal, "Modeling the appearance of special effect pigment coatings," *SPIE Surface Scattering and Diffraction for Advanced Metrology*, vol. 4447, pp. 77-86, 2001.
- [13] A. S. Glassner, *Principles of Digital Image Synthesis*: Morgan Kaufmann Publishers Inc., 1994.
- [14] S. Guy and C. Soler, "Graphics gems revisited: fast and physically-based rendering of gemstones," *ACM Trans. Graph.*, vol. 23, pp. 231-238, 2004.
- [15] X. D. He, K. E. Torrance, F. X. Sillion, and D. P. Greenberg, "A Comprehensive Physical Model for Light Reflection," *ACM SIGGRAPH Computer Graphics*, vol. 25, pp. 175-186, 1991.
- [16] D. S. Kliger, J. W. Lewis, and C. E. Randall, *Polarized Light in Optics and Spectroscopy*: Academic Press Inc, 1990.
- [17] A. Krishnaswamy, "Realistic Image Synthesis Engine (RISE), Open Source C++ Spectral Renderer," 2005.
- [18] M. I. Sancer, "Shadow-corrected electromagnetic scattering from a randomly rough surface," *IEEE Transactions on Antennas and Propagation*, vol. 17, pp. 577-585, 1969.
- [19] J. Stam, "Diffraction Shaders," *ACM SIGGRAPH Computer Graphics*, pp. 101-110, 1999.
- [20] D. C. Tannenbaum, P. Tannenbaum, and M. J. Wozny, "Polarization and Birefringency Considerations in Rendering," *Proceedings of SIGGRAPH 94*, pp. 221-222, 1994.
- [21] C. Ulbricht, A. Wilkie, and W. Purgathofer, "Verification of Physically Based Rendering Algorithms," *STAR Proceedings of Eurographics 2005*, pp. 95-112, 2005.
- [22] A. Wilkie, R. F. Tobler, and W. Purgathofer, "Combined Rendering of Polarization and Fluorescence Effects," *Proceedings of the 12th Eurographics Workshop on Rendering*, pp. 197-204, 2001.
- [23] A. Wilkie, R. F. Tobler, C. Ulbricht, G. Zotti, and W. Purgathofer, "An Analytical Model for Skylight Polarization," *Eurographics Symposium on Rendering*, pp. 387-399, 2004.
- [24] L. B. Wolff and D. Kurlander, "Ray Tracing with Polarization Parameters," *IEEE Computer Graphics & Applications*, vol. 10, pp. 44-55, 1990.

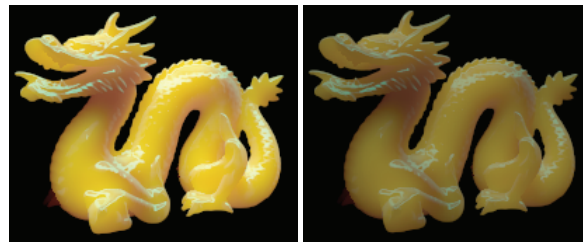


Figure 16a

Figure 16b

Figure 16. Illustrates the effects of polarization of surface and subsurface scattering from the rendered multilayered dragon statue using the new anisotropic theoretical reflectance model. Figure 16a is viewed without a polarized filter while Figure 16b is viewed through a polarizing filter.



Figure 17a

Figure 17b

Figure 17. Buddha statues that are made of a multilayered material simulated using the new anisotropic theoretical reflectance model. The image 17a was rendered without a polarized filter, while 17b was rendered with a polarizing filter.



Figure 18. Rendered Buddha statues made from jade. That was illuminated with by a light source that consists of 60% perpendicular and 40% parallel polarized using the isotropic reflectance model. The image on the left has the perpendicular polarized component removed as if it was viewed through a polarizing filter. While the image on the right has not undergone any filtering.

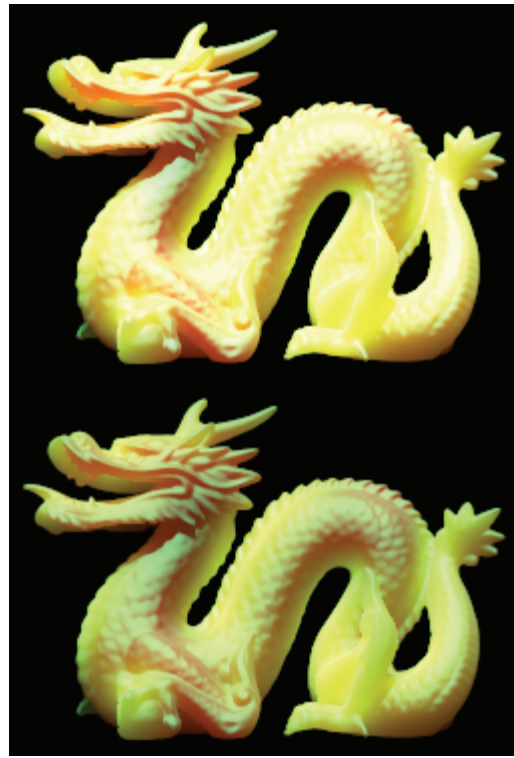


Figure 19. Illustrates the interaction of polarized light with a dragon statue coated with iridescent paint and illuminated with a D65 light source using the new anisotropic theoretical reflectance model. The top image is viewed without a polarized filter. The bottom image is viewed through a horizontal polarizing filter. For highly reflective dielectric materials the effects of glare can be great and the variation in the appearance and colour of the objects when viewed through the polarizing filter is noticeable compared to the image viewed without a polarizing filter.



Figure 20. A translucent dragon statue that is made of a type of nephrite jade that contains traces of manganese, simulated using the new anisotropic theoretical reflectance model